Journal of Computational Physics 228 (2009) 2239–2255

Contents lists available at ScienceDirect

Journal of Computational Physics

journal homepage: www.elsevier.com/locate/jcp

Numerical model reduction of 2D steady incompressible laminar flows: Application on the flow over a backward-facing step

Y. Rouizi [a], Y. Favennec [b,*,1], J. Ventura [a], D. Petit [a]

[a] LET UMR CNRS 6608, ENSMA – Université de Potiers - ESIP, Téléport 2, 1 Avenue Clément Ader, BP 40109, 86961 Futuroscope Cédex, France
[b] LET UMR CNRS 6608, ENSMA – Université de Potiers - ESIP, 40 Avenue du Recteur Pineau, Bâtiment de Mécanique, 86022 POITIERS Cédex, France

ARTICLE INFO

Article history:
Received 4 April 2008
Received in revised form 28 November 2008
Accepted 2 December 2008
Available online 14 December 2008

Keywords:
Model reduction
Identification method
Inverse problem of Parameter estimation
Optimization
Adjoint method

ABSTRACT

The numerical solution of most fluid mechanics problems usually needs such a fine mesh that the associated computational times become non-negligible parts in any design process. In order to couple numerical modelling schemes with inversion or control algorithms, the size of such models needs to be highly reduced. The identification method is a way to build low-order models that fit with the original ones. The laminar flow over a backward-facing step is used as a test case. Presented solutions are found to be in good agreement with experimental and numerical results found in the literature.

1. Introduction

Many industrial problems involve separating and reattaching flows in channels, usually combined with recirculation bubbles. Heat exchanger flows, for instance, often bear such kind of behaviors. But despite the complexity of the flow topology, the entire behavior of most fluid flows is described by the so-called Navier–Stokes equations.

Since in most cases, these equations do not provide the known analytical solutions, many numerical methods have been developed over the years to solve them. The space discretization can be based on, among others, the finite element formulation, or, more usually, the finite volume method.

Among the types of flows which ensure separation and recirculation bubbles, the one around a backward-facing step can be regarded as having a very simple geometry while retaining rich flow features like the ones mentioned above. The understanding of its structure may thus lead to a finer analysis of what may spring with more complex geometries. The backward-facing step flow has often been used as a test case to assess the accuracy and efficiency of the codes developed from the methods mentioned above. Indeed, its geometry does not prove to be challenging for meshing, and the experimental data are available in plenty.

The literature offers many numerical and experimental studies on 2D steady incompressible flows over the backward-facing step. Its topology is known to depend on geometrical parameters, but is still determined mostly by the Reynolds number. It is currently accepted that the flow features are stable and steady up to $Re = 800$, when this number is calculated on the upstream mean velocity and hydraulic diameter [1–4]. It can be noted that, still depending on the Reynolds number, the flow may exhibit one or two recirculation regions of varying lengths.

* Corresponding author. Tel.: +33 5 49 45 36 85.
E-mail address: Yann.Favennec@univ-nantes.fr (Y. Favennec).
[1] From September 2008, this author has been staying at Polytech' Nantes, Université de Nantes, La chantrerie - BP 50609, 44306 Nantes Cédex 3, France.

0021-9991/$ - see front matter © 2008 Elsevier Inc. All rights reserved.
doi:10.1016/j.jcp.2008.12.001

Any discretization method leads to the resolution of a matrix system of algebraic equations (AEs), instead of the integration of continuous partial differential equations (PDEs). For the solution of the matricial system to be close enough to the solution of the partial differential equations, the time-space discretization must be fine enough. This constraint usually leads to large matricial systems. Thus, depending on the mesh size and on the physics to be approximated, the computational price to pay to obtain a suitable solution can be high in terms of memory and CPU time.

When the solution of the model is to be found several times for particular applications, e.g. for inverse or optimization problems, then one has to re-assess the compromise made between accuracy and time consumption. One way to avoid the loss of accuracy is to consider reduction modeling techniques. These methods aim to solve a restricted number n of ordinary differential equations (ODEs) instead of the $N \gg n$ equations given by the "classical" discretization of the partial differential equations.

When considering reduction techniques, one may cite the methods using a basis change [5] reduction in the physical space of variables. For thermal linear problems, several methods coming from automatics have been successfully applied [6]. Though many reduction methods for application on linear systems exist, a few of them are viable for applications on nonlinear problems. On the one hand, the Proper Orthogonal Method coupled with the Galerkin projection (POD-G) has proved to be very efficient on fluid-type nonlinear problems where turbulence plays a non-negligible role [7–9]. On the other hand, the Modal Identification Method (MIM) has proved to be very efficient on diffusion-type nonlinear problems [10–12]. A comparison on a particular nonlinear diffusive problem between both the POD-Galerkin method and the Modal Identification Method recently proved that both methods are accurate and robust and that both can be formulated equivalently although the general ideas behind those two are completely different [13].

In this paper, a method derived from the Modal Identification Method is used to identify some reduced models related to some fluid mechanics problems. The reduction process leans on the solution of an inverse problem of parameter estimation: one defines the structure of the reduced model formulation before estimating the related vectors and matrices through the solution of an optimization problem. Let us insist here on an important point: the identification method aims at reproducing data that are supposed to be well described by the temporal equations of the detailed model, which is then a reference. Thus, when deriving the detailed model directly out of the Navier–Stokes equations, we ensure that we can use fields coming from any numerical codes, as long as those fields are a good approximation of a Navier–Stokes solution. It implies that the formulation of the reduced model is independent of the numerical code which provides the data to be used. It does not even depend on the class of numerical schemes used (e.g. finite differences and finite volume). The reduction method can even be used based on the experimental data. Consequently, the actual purpose of this paper is to evaluate the ability of the reduced model to reproduce and to predict the results obtained by a numerical code solving the Navier–Stokes equations. For reasons of simplicity and also because it is a very well-known code among fluid mechanics engineers, we chose to use the finite-volume code Fluent 6.3.26 to provide us with the flow data.

The developed identification method leads to consider some low-order models that are related to some high-order models. In this sense, one can speak of model reduction. Also, since the approach leans upon an optimization algorithm, one can also speak of compact modeling coupled with data fitting, sometimes referred as behavioural modeling. Actually, due to the fact that the matrices of the reduced models are not computed in direct way but rather identified in the modal form, one uses the terminology "modal identification method for model reduction".

This paper is organized as follows: In Section 2, the formulation of the detailed model is derived. The governing Navier–Stokes equations together with the boundary conditions are given. The variational problem is considered along with the special treatment of the pressure variable and the boundary conditions. This section, based upon the classical literature, e.g. [14,15] and also [16,17], eventually gives a formulation that is suitable for model reduction through the identification method. Note again that this formulation is not necessarily the one that is used to obtain the data before the estimation of the reduced model. Next, Section 3 gives the main keys for model reduction through the identification method. We detail there the reduced model formulation and its identification, which leans on the use of optimization algorithms. More precisely, one uses a gradient-type method where the gradient of the cost function is computed through the adjoint problem. In Section 4, we present some numerical results of model reduction for the backward-facing step problem. We find that the developed identification method seems to be well suited for model reduction in this particular but representative case. Eventually, Section 5 is dedicated to some conclusions and especially to future prospective works.

2. Formulation of the structure of the detailed model designed for model reduction

2.1. The governing equations

Let Ω be an open-bounded domain in $\mathbb{R}^d$, $(d = 2, 3)$, with a boundary $\partial\Omega$ and an outward pointing normal $\boldsymbol{n}$. For $T > 0$, we consider the problem of solving, for $\boldsymbol{u} : \Omega \times (0,T) \to \mathbb{R}^d$ and $p : \Omega \times (0,T) \to \mathbb{R}$, the time-dependent Navier–Stokes equations:

$$\begin{cases} \frac{\partial \boldsymbol{u}}{\partial t} + (\boldsymbol{u} \cdot \nabla)\boldsymbol{u} - \nu \Delta \boldsymbol{u} + \frac{1}{\rho}\nabla p = 0 & \text{in } \Omega \times (0,T), \\ \nabla \cdot \boldsymbol{u} = 0 & \text{in } \Omega \times (0,T), \end{cases} \tag{1}$$

where $\boldsymbol{u}(\boldsymbol{x},t)$ is the flow velocity, $p(\boldsymbol{x},t)$ is the pressure, $\nu > 0$ is the kinematic viscosity of the fluid, $\rho > 0$ is the fluid density and $\boldsymbol{x}$ is the collection of $(x_i), i = 1, \ldots, d$.

The characteristics of the flow depend on some nondimensional parameters, essentially on the Reynolds number $Re = \tilde{u}\ell/\nu$, where $\tilde{u}$ is a characteristic velocity, and ℓ is a characteristic length.

When considering time-dependent problems, an initial condition has also to be considered. This is of the type

$$\boldsymbol{u}(\boldsymbol{x}, 0) = \boldsymbol{u}_0(\boldsymbol{x}) \quad \text{in } \Omega, \tag{2}$$

where $\boldsymbol{u}_0 \in [L^2(\Omega)]^d$.

2.2. The boundary conditions

In the following application, several types of boundary conditions may be applied to model the fluid adherence on a fixed boundary along with a fixed input flux, a free output flux, and a possibly symmetry boundary condition. We introduce the following system defining the set of boundary conditions:

$$\boldsymbol{u} = \bar{\boldsymbol{u}} \quad \text{on } \partial\Omega_1, \tag{3a}$$
$$-\nu\nabla\boldsymbol{u}\cdot\boldsymbol{n} + p\boldsymbol{n} = 0 \quad \text{on } \partial\Omega_2, \tag{3b}$$
$$\boldsymbol{u}\cdot\boldsymbol{n} = 0 \quad \text{on } \partial\Omega_3, \tag{3c}$$
$$(\nabla\boldsymbol{u}\cdot\boldsymbol{n})\cdot\boldsymbol{\tau}_i = 0 \quad i = 1,\ldots,d-1 \quad \text{on } \partial\Omega_3, \tag{3d}$$

where $\{\partial\Omega_1, \partial\Omega_2, \partial\Omega_3\}$ forms a partition of $\partial\Omega$, $\boldsymbol{n}$ and $\boldsymbol{\tau}_i$ are, respectively, the normal unit vector and the tangential unit vectors to $\partial\Omega$.

2.3. The variational formulation

For sufficiently regular functions $\boldsymbol{u}$ and p, the problem (1) becomes

Find $\boldsymbol{u}(\boldsymbol{x}, t), p(\boldsymbol{x}, t)$ such that

$$\begin{cases} \frac{d}{dt}(\boldsymbol{u}, \boldsymbol{v})_\Omega + a(\boldsymbol{u}, \boldsymbol{v}) + b(\boldsymbol{u}; \boldsymbol{u}, \boldsymbol{v}) + c(\boldsymbol{v}, p) = 0 & \forall \boldsymbol{v} \in \boldsymbol{V}, \\ c_0(\boldsymbol{u}, q) = 0 & \forall q \in Q, \\ +\text{essential boundary conditions} \end{cases} \tag{4}$$

where [14]

- $\boldsymbol{V} \subset [W^{1,2}(\Omega)]^d$, with the Sobolev space $W^{1,p}(\Omega)$ defined as

$$W^{1,p}(\Omega) = \left\{ u \in L^p(\Omega) \middle| \frac{\partial u}{\partial x_j} \in L^p(\Omega) \text{ for } j = 1,\ldots,d \right\},$$

equipped with the norm

$$\|u\|_{W^{1,p}(\Omega)} = \left(\int_\Omega \left(\frac{1}{\lambda^p}|u|^p + \sum_{j=1}^{d} \left| \frac{\partial u}{\partial x_j} \right|^p \right) d\boldsymbol{x} \right)^{\frac{1}{p}},$$

where λ is a characteristic length (often taken equal to 1). Note that vector-valued counterparts of scalar spaces are denoted by bold-face symbols, e.g., $\boldsymbol{H}^1(\Omega) = [H^1(\Omega)^d]$;
- $Q \subset L^2(\Omega)$ is the collection of square-integrable functions defined on Ω;
- $(\cdot,\cdot)_\Omega$ is the inner product of $L^2(\Omega)$;
- $a = a_0 + a_1$;
- $a_0 : \boldsymbol{V} \times \boldsymbol{V} \to \mathbb{R}$ is the bilinear continuous and coercive form

$$a_0(\boldsymbol{u}, \boldsymbol{v}) = \nu(\nabla\boldsymbol{u}, \nabla\mathbf{v})_\Omega,$$

- $a_1 : \boldsymbol{V} \times \boldsymbol{V} \to \mathbb{R}$ is the bilinear form

$$a_1(\boldsymbol{u}, \boldsymbol{v}) = -\nu(\nabla\boldsymbol{u}\cdot\boldsymbol{n}, \mathbf{v})_{\partial\Omega},$$

- $b : \boldsymbol{V} \times \boldsymbol{V} \times \boldsymbol{V} \to \mathbb{R}$ is the trilinear form given by

$$b(\boldsymbol{u}; \boldsymbol{v}, \boldsymbol{w}) = \sum_{i,j=1}^{d} \int_\Omega u_i \frac{\partial v_j}{\partial x_i} w_j,$$

where u_i, v_i and w_i are the canonical components of $\boldsymbol{u}$, $\boldsymbol{v}$ and $\boldsymbol{w}$, respectively;
- $c = \frac{1}{\rho}(c_0 + c_1)$;
- $c_0 : \boldsymbol{V} \times Q \to \mathbb{R}$ is the continuous bilinear form given by

$$c_0(\boldsymbol{v}, q) = -(\nabla\cdot\boldsymbol{v}, q)_\Omega,$$

- and $c_1 : \boldsymbol{V} \times Q \to \mathbb{R}$ is the continuous bilinear form given by

$$c_1(\boldsymbol{v}, q) = (\boldsymbol{v} \cdot \boldsymbol{n}, q)_{\partial\Omega}.$$

When considering the boundary conditions (3d), we have [15]

$$\boldsymbol{V} = \left\{ \boldsymbol{v} \in H^1(\Omega)^d | \boldsymbol{v} = 0 \quad \text{on } \partial\Omega_1 \; \boldsymbol{v}.\boldsymbol{n} = 0 \quad \text{on } \partial\Omega_3 \right\},$$

$$Q = \begin{cases} L^2_0(\Omega) = \left\{ q \in L^2(\Omega) \middle| \int_\Omega q(\boldsymbol{x}) d\boldsymbol{x} = 0 \right\} & \text{if } \partial\Omega_2 = \varnothing, \\ L^2(\Omega) & \text{if } \partial\Omega_2 \neq \varnothing. \end{cases}$$

Let us point out that while both conditions (3b) and (3d) are the natural boundary conditions normally present in the variational formulation, both essential boundary conditions (3a) and (3c) still need to be integrated to the form (4).

Note also that other kinds of variational formulation can be formulated. For instance, when considering the divergence-free subspace of $\boldsymbol{V} : \boldsymbol{V}_0 = \{\boldsymbol{v} \in \boldsymbol{V} : \nabla \cdot \boldsymbol{v} = 0\}$ introduced by Hecht (see [15,18] for instance), the variational problem (4) simplifies to "Find $\boldsymbol{u}(\boldsymbol{x}, t)$ such that $(\partial_t \boldsymbol{u}, \boldsymbol{v})_\Omega + a(\boldsymbol{u}, \boldsymbol{v}) + b(\boldsymbol{u}; \boldsymbol{u}, \boldsymbol{v}) = 0 \; \forall \boldsymbol{v} \in \boldsymbol{V}_0 +$ essential boundary conditions". We, however, continue the derivation with the formulation (4).

2.4. Space semi-discretization

In this section, we introduce a finite element discretization of (4). For simplicity, we will state the results by assuming $\Omega_h = \Omega$, where Ω_h is the approximate domain on which the finite-dimensional function spaces are defined on. Denoting V_h the space of continuous piecewise polynomial function (for instance, V_h^k if functions of degree k) and $Q_h = V_h \cap L^2_0(\Omega)$, and denoting $\boldsymbol{W}_h = [V_h]^d \times Q_h$ our space semi-discretized scheme reads: for all $t \in (0, T)$, find $(\boldsymbol{u}_h(t), p_h(t)) \in \boldsymbol{W}_h$ such that

$$\begin{cases} (\partial_t \boldsymbol{u}_h, \boldsymbol{v}_h)_{\Omega_h} + a(\boldsymbol{u}_h, \boldsymbol{v}_h) + b(\boldsymbol{u}_h; \boldsymbol{u}_h, \boldsymbol{v}_h) + c(\boldsymbol{v}_h, p_h) = 0, \\ c_0(\boldsymbol{u}_h, q_h) = 0 \end{cases}$$

for all $(\boldsymbol{v}_h, q_h) \in \boldsymbol{W}_h$ and with $\boldsymbol{u}_{0_h}$ a suitable approximation of $\boldsymbol{u}_0$ in $[V_h]^d$. The projection of this space semi-discretized formulation onto the finite element bases $\boldsymbol{\varphi}_i(x)$, $i = 1, \ldots, p$ and $\psi_i(x)$, $i = 1, \ldots, q$ gives

$$\begin{cases} \left(\boldsymbol{\varphi}_i, \boldsymbol{\varphi}_j\right)_{\Omega_h} \frac{d\tilde{\boldsymbol{u}}_j}{dt} + a\left(\boldsymbol{\varphi}_i, \boldsymbol{\varphi}_j\right)\tilde{\boldsymbol{u}}_j + \tilde{\boldsymbol{u}}_k b\left(\boldsymbol{\varphi}_k; \boldsymbol{\varphi}_i, \boldsymbol{\varphi}_j\right)\tilde{\boldsymbol{u}}_j + c\left(\boldsymbol{\varphi}_i, \psi_j\right)\tilde{p}_j = 0 \quad \forall i = 1, \ldots, p, \\ \tilde{\boldsymbol{u}}_i^t c_0\left(\boldsymbol{\varphi}_i, \psi_j\right) = 0 \quad \forall j = 1, \ldots, q, \end{cases}$$

where the summation Einstein convention is used with $j = 1, \ldots, p$ and $k = 1, \ldots, p$ for the first equation and $i = 1, \ldots, p$ for the second equation. This projected formulation can be written in matrix form such that the problem consists now in finding for all $t \in (0, T)$: $(\tilde{\boldsymbol{u}}, \tilde{p}) \in \mathbb{R}^{\dim(\boldsymbol{V}_h) + \dim(Q_h)}$ such that

$$\begin{cases} \mathcal{M}_{i,j} \frac{d\tilde{\boldsymbol{u}}_j}{dt} + \mathcal{A}_{i,j}\tilde{\boldsymbol{u}}_j + \tilde{\boldsymbol{u}}_k \mathcal{B}_{k,i,j}\tilde{\boldsymbol{u}}_j + \mathcal{C}_{i,j}\tilde{p}_j = 0 \quad \forall i = 1, \ldots, p, \\ \mathcal{C}_{0j,i}\tilde{\boldsymbol{u}}_i = 0 \quad \forall j = 1, \ldots, q. \end{cases} \tag{5}$$

2.5. The pressure treatment

The system (5) is written in terms of semi-discretized velocities $\tilde{\boldsymbol{u}}$ and pressure $\tilde{p}$. A large number of methods may be used to solve the coupled system based on the time integration of (5). The coupled Uzawa and conjugate gradient algorithm for instance [19,20], or the Chorin's projection scheme [15] is proved to be very efficient for solving many Navier–Stokes problems.

The use of such projection algorithms leads to consider a coupled problem between velocities and pressure. Within the area of model order reduction, structure preserving methods have been developed in the recent years that can cope with two types of variables [21,22]. However, due to the identification method presented further, the coupling formulation is not the most appropriate and especially easy-to-use formulation. We thus rather consider the method which consists in taking the divergence of the first relationship of (1)

$$\nabla \cdot \left(\frac{\partial \boldsymbol{u}}{\partial t} + (\boldsymbol{u} \cdot \nabla)\boldsymbol{u} - \nu \Delta \boldsymbol{u} + \frac{1}{\rho} \nabla p \right) = \frac{\partial}{\partial t}(\nabla \cdot \boldsymbol{u}) + \nabla \cdot ((\boldsymbol{u} \cdot \nabla)\boldsymbol{u}) - \nu \Delta(\nabla \cdot \boldsymbol{u}) + \frac{1}{\rho} \Delta p = \nabla \cdot ((\boldsymbol{u} \cdot \nabla)\boldsymbol{u}) + \frac{1}{\rho} \Delta p = 0,$$

where one has used $\nabla \cdot \boldsymbol{u} = 0$ for simplifying the divergence of the nonlinear term. The pressure equation then writes

$$\Delta p = -\rho \nabla \cdot ((\boldsymbol{u} \cdot \nabla)\boldsymbol{u}) = -\rho \sum_{i,j=1}^{d} \frac{\partial u_i}{\partial x_j} \frac{\partial u_j}{\partial x_i}, \tag{6}$$

which is easy to solve with adequate boundary conditions for the pressure p (see for instance [15,23] for different conditions). Choosing $p \in Q$ with $\bar{p} \in \{\bar{p} \in L^2(\Omega) | \bar{p} = 0 \text{ on } \partial\Omega\}$, the weak form of (6) reads

$$a_0(p, \bar{p}) + \nu d(\boldsymbol{u}; \boldsymbol{u}, \bar{p}) = 0,$$

where

$$d(\boldsymbol{u};\boldsymbol{v},\bar{p}) = \rho \sum_{i,j=1}^{d} \int_{\Omega} \frac{\partial u_i}{\partial x_j}\frac{\partial v_j}{\partial x_i}\bar{p}.$$

The projection of the space-discretized version of this equation onto the finite element basis $\psi_i(x), i = 1,\ldots,q$ and $\boldsymbol{\varphi}_i(x), i = 1,\ldots,p$ gives:

$$a_0(\psi_i,\psi_j)\tilde{p}_j + \nu\tilde{\boldsymbol{u}}_k d(\boldsymbol{\varphi}_k;\boldsymbol{\varphi}_j,\psi_i)\tilde{\boldsymbol{u}}_j,$$

which corresponds in a matrix form to

$$\mathcal{D}_{i,j}\tilde{p}_j + \tilde{\boldsymbol{u}}_k\mathcal{E}_{k,i,j}\tilde{\boldsymbol{u}}_j = 0. \tag{7}$$

The introduction of (7) into (5a) gives eventually, using $\mathcal{B} \leftarrow \mathcal{B} - \mathcal{C}\mathcal{D}^{-1}\mathcal{E}$

$$\mathcal{M}_{i,j}\frac{d\tilde{\boldsymbol{u}}_j}{dt} + \mathcal{A}_{i,j}\tilde{\boldsymbol{u}}_j + \tilde{\boldsymbol{u}}_k\mathcal{B}_{k,i,j}\tilde{\boldsymbol{u}}_j = 0 \quad \forall i = 1,\ldots,p.$$

Though the introduction of the pressure equation into the velocity equation through this way is likely to be inefficient for a detailed modeling, this obtained formulation is regarded as being suitable for model reduction. The nonlinear equation given above can be rewritten in a compact form as

$$\left(\frac{d}{dt} + \mathcal{L} + \mathcal{Q}\right)(\tilde{\boldsymbol{u}}) = 0, \tag{8}$$

where the linear operator is given by $\mathcal{L}(\boldsymbol{v}) = \mathcal{M}^{-1}\mathcal{A}\boldsymbol{v}$ and where the quadratic operator is given by $\mathcal{Q}(\boldsymbol{v}) = \mathcal{M}^{-1}\mathcal{B}\boldsymbol{v}\otimes\boldsymbol{v}$.

2.6. Dirichlet boundary conditions

While natural boundary conditions are taken into account in (8), the essential boundary conditions still have to be integrated into (8). The system to be dealt with contains actually (8) coupled with

$$\mathcal{G}(\tilde{\boldsymbol{u}}) = h, \tag{9}$$

where $\mathcal{G}(\boldsymbol{v}) = \boldsymbol{v}$ and $h = \bar{\boldsymbol{u}}$ when considering nodes on $\partial\Omega_1$ and where $\mathcal{G}(\boldsymbol{v}) = \boldsymbol{v}\cdot\boldsymbol{n}$ and $h = 0$ when considering nodes on $\partial\Omega_3$.

A common method to solve the coupled problem (8) and (9) consists in solving the optimization problem

$$\inf_{\tilde{u}\in\boldsymbol{V}_{\mathbf{h}}}\left\{\left\|\left(\frac{d}{dt} + \mathcal{L} + \mathcal{Q}\right)(\tilde{\boldsymbol{u}})\right\|^2 + \|\mathcal{G}(\tilde{u}) - h\|^2\right\}$$

with appropriate norms for each term. Another method more suitable for finding a formulation designed for model reduction consists in applying exactly the essential boundary conditions. The time integration of (8) gives, when linearized

$$\mathcal{A}\boldsymbol{u}^n = \mathcal{B} \quad \forall n \in \mathbb{N}^*,$$

where the superscript n stands for the time $t_n = n\times\delta t$. In this time-integrated equation, $\mathcal{A} = [\mathbb{I} + \delta t(\mathcal{L} + \mathcal{Q})]$ and $\mathcal{B} = \boldsymbol{u}^{n-1}$ for instance if an implicit time integration scheme is considered. The use of some other schemes would not change drastically the derivation of the problem. Let us prescribe the condition $\boldsymbol{u} = \bar{\boldsymbol{u}}$ on the kth node (i.e. $\boldsymbol{x}(P_k)\in\partial\Omega_1$). The system above is then changed to

$$\mathcal{A}\boldsymbol{u}^n = \mathcal{B} - \mathcal{A}_k\bar{\boldsymbol{u}},$$

(where $\mathcal{A}_k$ stands for the vector representing the kth column of $\mathcal{A}$) before the kth row of the matrix system (along with the kth column of $\mathcal{A}$) is removed, reducing the size of the system by a unit order. This procedure is repeated for all the nodes where a Dirichlet condition is prescribed on. The system above thus becomes

$$\tilde{\mathcal{A}}\tilde{\boldsymbol{u}}^n = \tilde{\mathcal{B}} - \sum_{i|\boldsymbol{x}(P_i)\in\partial\Omega_1}\mathcal{A}_i\bar{\boldsymbol{u}}(\boldsymbol{x}_i), \tag{10}$$

where $\tilde{\mathcal{A}}$ is the matrix $\mathcal{A}$ without the ith lines and ith columns and $\tilde{\mathcal{B}}$ is the matrix $\mathcal{B}$ without the ith lines, i.e. corresponding to $\boldsymbol{x}(P_i)\in\partial\Omega_1$.

This method applied on, for instance, the implicit time integration scheme gives

$$\left[\tilde{\mathbb{I}} + \delta t(\tilde{\mathcal{L}} + \tilde{\mathcal{Q}})\right](\tilde{\boldsymbol{u}}^n) = \tilde{\boldsymbol{u}}^{n-1} - \sum_i \mathcal{A}_i\bar{\boldsymbol{u}}(\boldsymbol{x}_i),$$

which corresponds in a time-continuous form to

$$\left(\frac{d}{dt} + \tilde{\mathcal{L}} + \tilde{\mathcal{Q}}\right)(\tilde{\boldsymbol{u}}) = \mathcal{D}(\bar{\boldsymbol{u}}). \tag{11}$$

3. Model reduction

Let us rewrite (11) in a form that is more suitable for model reduction:

$$\frac{d\boldsymbol{u}}{dt} = A\boldsymbol{u} + \Psi(\boldsymbol{u}) + B\bar{\boldsymbol{u}} + B^{+}, \tag{12}$$

where $A\boldsymbol{u} = -\tilde{\mathcal{L}}(\boldsymbol{u})$, $\Psi(\mathbf{u}) = -\tilde{\mathcal{Q}}(\boldsymbol{u})$, $\bar{\boldsymbol{u}}$ represents the prescribed boundary conditions used as input data for reduction and B is thus the input matrix, and B^{+} represents other input data, e.g. some Dirichlet boundary conditions or fluxes not taken into account as expressed input (one has $\mathcal{D}(v) = Bv + B^{+}$).

Let us also introduce the output relationship which enables to select a part of the computed field:

$$Y = C\boldsymbol{u}, \tag{13}$$

where one uses the partition $Y_{u_i} = C_{u_i}u_i$, $i = 1, \ldots, d$. Relationships (12) and (13) make up the so-called detailed model expressed in a form suitable for reduction.

The idea behind model reduction is to find an equivalent model but with fewer degrees of freedom. In fluid mechanics problems, the POD-Galerkin method has proved to be very efficient when considering turbulent flows [7–9,18]. On the other hand, for transient problems such as diffusive problems, the modal identification method has proved to reproduce with accuracy the behavior of systems even taking into account of the complex boundary conditions [12]. In addition, some comparisons have been performed between both cited methods on a purely diffusive test case [13]. This study showed that both methods are powerful in terms of accuracy and order reduction, but with a slight advantage for the modal identification method. The goal is here to use an identification method just derived from the modal identification method. Note that while the identification method has been successfully applied on the $(\Psi - \omega)$ variables [24] for the lid-driven cavity and for 2D pipe flows, the problem is here treated through the use of primal variables, i.e. velocities.

3.1. The reduced model formulation

Let Λ be the diagonal matrix of A involved in (12) and Σ the matrix of eigenvectors of A such that $\Lambda = \Sigma^{-1}A\Sigma$, and let perform the change of variable $\boldsymbol{u} = \Sigma X$, $X \in \mathbb{R}^{d\times N}$ where N is the number of degrees of freedom involved in (12). Then (12) becomes

$$\frac{dX}{dt} = \Lambda X + \Sigma^{-1}\Psi(\Sigma X) + G\bar{\boldsymbol{u}} + G^{+},$$

where $G = \Sigma^{-1}B$, $G^{+} = \Sigma^{-1}B^{+}$ and the output equation is now expressed with $Y = C\Sigma X = HX$. The quadratic term $\Sigma^{-1}\Psi(\Sigma X)$ may be reformulated to $\Omega Z(X)$, where $\Omega \in \mathbb{R}^{(d\times N, \dim(Z)(d\times N))}$ and $Z(X)$ is a vector containing the crossed products

$$X_iX_j \quad \text{with} \begin{cases} i,j = 1, \ldots, d\times N, \\ i \leqslant j, \end{cases}$$

and $\dim(Z)(m) = m(m+1)/2$. The model is thus written as

$$\begin{cases} \frac{dX}{dt} = \Lambda X + \Omega Z(X) + G\bar{\boldsymbol{u}} + G^{+}, \\ Y = HX. \end{cases}$$

When considering time-independent problems, the problem above becomes

$$\begin{cases} X + \Omega Z(X) + G\bar{\boldsymbol{u}} + G^{+} = 0, \\ Y - HX = 0, \end{cases} \tag{14}$$

where we used $\Omega \leftarrow \Lambda^{-1}\Omega$, $G \leftarrow \Lambda^{-1}G$ and $G^{+} \leftarrow \Lambda^{-1}G^{+}$.

The formulation (14) leads to solve a system of $d \times N$ equations, N being related to the space discretization. In the developed identification method, we use this formulation as the structure for the model that has to be identified. The reduction procedure is thus relative to a new state x such that $\dim x \ll \dim X$. Hence, the reduced model structure is, with $\widetilde{Y}$ the approximation of Y

$$x + \omega Z(x) + g\bar{\boldsymbol{u}} + g^{+} = 0, \tag{15a}$$

$$\widetilde{Y} - hx = 0. \tag{15b}$$

The problem thus consists in finding the matrix $\omega \in \mathbb{R}^{(n,\dim(Z)(n))}$, the input matrix $g \in \mathbb{R}^{n\times p}$, the additional vector $g^{+} \in \mathbb{R}^{n}$ and the output matrix $h \in \mathbb{R}^{q\times n}$ involved in the general reduced model formulation (15b). The size of the input matrix g depends on both the reduced model order n and q, which is the number of nodes element of the boundary $\partial\Omega_1$ where a non-null Dirichlet condition is prescribed. Note that the passage from (14) to (15b) leads to consider very low-order models of size $n \ll \dim(X) = d \times N$. Note also that the number n is completely independent on the considered geometry and is even independent on the 1D, 2D or 3D geometry characteristics.

3.2. The reduced model identification

The evaluation of vectors and matrices involved in (15b) may be computed in the straightforward way from (12) and (13) solving the eigenvalue problem and selecting the most dominant modes. The other way consists in identifying all the components involved in (15b) through the solution of the optimization problem:

$$\inf_{\beta\in\mathcal{B}} j(\beta), \tag{16}$$

where β is the collection of $\omega_{i,j}$, $g_{i,k}$, g_i^+ and $h_{l,i}$ with $i = 1,\dots,m$ (m being the reduced model order), $j = 1,\dots,\dim(Z)(m)$, $k = 1,\dots,p$ (p being the number of input) and $l = 1,\dots,q$ (q being the number of location output), and $\mathcal{B} = \mathbb{R}^{\dim(\beta)}$. The cost function j to be minimized is based on a quadratic norm of errors between the output $\widetilde{Y}$ given by the reduced model and the output Y^* given by a detailed model. This norm is integrated on all performed comparisons ($k = 1,\dots,K$), hence

$$j(\beta) = \mathcal{J}(x,\beta) = \sum_{k=1}^{K} (Hx - Y^*, Hx - Y^*), \tag{17}$$

where $(\cdot,\cdot)$ is the inner product in $\mathcal{Y}$.

The solution of the optimization problem is performed iteratively with an outer loop incrementing the reduced model order and an inner loop solving effectively (16). Algorithm 1 presents schematically the procedure that is used for model reduction through identification. In there, the satisfactory results evoked in steps (3f) and (4) are related to some criteria defined and discussed in [11].

The optimization being non-purely quadratic, an iterative procedure is used to converge to the solution $\bar{v} = \arg\min_{v\in\mathcal{B}} j(v)$. The quasi-Newton B.F.G.S algorithm is used [25]. At each iteration, the reduced model (15b) is integrated, the cost function is computed, and the cost gradient is computed integrating an adjoint problem.

Algorithm 1. The reduced model identification algorithm

(1) Form the output Y^* through either the solution of K detailed models or from K experiments
(2) Let $m = 1 \setminus\setminus m = \dim x$
(3) $\ell = 0$, initialize $\omega = \omega_m^0$, $g = g_m^0$
  (a) Compute the reduce model to get x;
  (b) Identify the matrix h through the minimization of the quadratic norm of $h\chi - \Upsilon$ where χ is the collection of x and Υ is the collection of Y^* for $k = 1,\dots,K$, i.e. through $h^t = (\chi\cdot\chi^t)^{-1}\chi\Upsilon^t$;
  (c) Compute the cost function $\mathcal{J}$ from the solution of the "direct" reduced model (15b) with ω_m^ℓ and g_m^ℓ;
  (d) Compute the adjoint model and the cost function gradient (26)
  (e) Compute the new parameters from a gradient-type algorithm (as far as we are concerned we use the BFGS quasi-Newton algorithm [25]);
  (f) If satisfactory result: end, else $\ell \leftarrow \ell + 1$ and return to step 3a.
(4) If satisfactory result: end, else $m \leftarrow m + 1$ and return to step 3.

The objective function gradient is obtained in the following way [26,27]. The directional derivative of $\mathcal{J}$ towards δw is defined when the limit (18) exists:

$$\widehat{\mathcal{J}}(x,\beta,\delta w) = \lim_{\epsilon\to 0} \frac{\mathcal{J}(x,\beta+\epsilon\delta w) - \mathcal{J}(x,\beta)}{\epsilon}, \tag{18}$$

where the tuning parameter ϵ is the finite-difference interval. Even though the Finite Difference Method is easy to implement, it has the disadvantage of being highly CPU time consuming. Indeed, the method needs as many integrations of the model given by (15b) as the number of parameters. Moreover, the value for ϵ has to be chosen within a region where variables depend roughly linearly on ϵ. Indeed for too small values, the round-off errors dominate while for too high values one gets a nonlinear behavior. The objective function directional derivative is also obtained by differentiating (17):

$$\widehat{\mathcal{J}}(x,\beta,\delta w) = \left(\frac{\partial\mathcal{J}}{\partial x},\hat{x}\right) + \left(\frac{\partial\mathcal{J}}{\partial\beta},\delta w\right), \tag{19}$$

where $\hat{x}$ is the directional derivative of x in the direction δw and where $(\cdot,\cdot)$ stands for the inner products $(\cdot,\cdot)_{\mathcal{W}}$ and $(\cdot,\cdot)_{\mathcal{B}}$ associated to the norm $\|\cdot\|_{\mathcal{Y}} = (\cdot,\cdot)_{\mathcal{Y}}^{1/2}$. One then computes the directional derivative of the direct model (15b) in the direction δw to access the "sensitivity" problem:

$$\frac{\partial\mathcal{R}}{\partial\beta}\times\delta w + \left(\mathbb{I}_m + \omega\widetilde{Z}\right)\times\hat{x} = 0, \tag{20}$$

where $\mathbb{I}_m$ is the identity matrix of order m, $\mathcal{R}$ represents the residue of the model (15a), $\frac{\partial\mathcal{R}}{\partial\beta}$ is the jacobian of $\mathcal{R}$ with respect to β and $\widetilde{Z}$ is the jacobian of Z with respect to the reduced state x. Note that we have also by definition:

$$(\nabla j(\beta),\delta w) = \left(\frac{\partial\mathcal{J}}{\partial x},\hat{x}\right) + \left(\frac{\partial\mathcal{J}}{\partial\beta},\delta w\right), \tag{21}$$

and, taking into account of (17):

$$(\nabla j(\beta), \delta w) = \sum_{k=1}^{K} \left(H^t(Hx - Y^*), \hat{x}\right). \tag{22}$$

Using δw as the canonical directions of β, all the components of $\nabla j(\beta)$ can be computed from the solution of (20) and then performing the scalar product (22). This method, called the direct differentiation method is, however, highly time consuming since one direct linear sensitivity problem has to be solved to access each component of the gradient.

The objective function gradient is obtained by taking advantage of the linear dependence of $(\nabla j(\beta), \delta w)$ with respect to δw. This is done by introducing the adjoint variable $\lambda \in \mathbb{R}^{\dim(x)}$. Taking the inner product of (20) with λ gives

$$\left(\frac{\partial \mathcal{R}}{\partial \beta} \times \delta w, \lambda\right) + \left(\left(\mathbb{I}_m + \omega \widetilde{Z}\right) \times \hat{x}, \lambda\right) = 0, \tag{23}$$

and transposing we get

$$\left(\delta w, \left(\frac{\partial \mathcal{R}}{\partial \beta}\right)^t \times \lambda\right) + \left(\hat{x}, \left(\mathbb{I}_m + \widetilde{Z}^t \omega^t\right) \times \lambda\right) = 0. \tag{24}$$

Eventually, using (21), if the adjoint is defined as the solution of the adjoint model:

$$\left(\mathbb{I}_m + \widetilde{Z}^t \omega^t\right) \times \lambda = \sum_{k=1}^{K} H^t(Hx - Y^*), \tag{25}$$

then we obtain the gradient:

$$\nabla j(\beta) = -\left(\frac{\partial \mathcal{R}}{\partial \beta}\right)^t \times \lambda,$$

that is also

$$\nabla j = \left((Z_j, \lambda_i)_{\substack{i=1,\dots,m \\ j=1,\dots,\dim(Z)(m)}}, (\bar{\boldsymbol{u}}_k, \lambda_i)_{\substack{i=1,\dots,m \\ k=1,\dots,p,}} (1, \lambda_i)_{i=1,\dots,m} \right)^t, \tag{26}$$

the different blocks being related to the components of the cost function gradient with respect to $\omega_{i,j}$, $g_{i,k}$ and g_i^+, respectively.

Note that the components of the observation matrix h are not included in (26) because since there is a linear relationship between the output $\widetilde{Y}$ and the state x via h, then the least squares method can be employed for the identification of h at lower costs (see Algorithm 1 and especially [28] for more explanation).

In the general way [26,29], the gradient is computed by solving the adjoint problem (25) to calculate the adjoint variable λ, and then by applying the gradient relationship (26). Note that the adjoint variable λ (also called the co-state variable) has the meaning of a Lagrange multiplier when considering the Lagrange function $\mathcal{L} : \mathcal{W} \times \mathcal{B} \times \mathbb{R}^{\dim(x)} \mapsto \mathbb{R}$ defined by $\mathcal{L}(x, \beta, \lambda) = \mathcal{J}(x, \beta) + \lambda \cdot (x + \omega Z(x) + g\bar{\boldsymbol{u}} + g^+)$ where the direct state Eq. (15a) is penalized [26,30].

4. Model reduction on the backward-facing step

4.1. The physical problem and the detailed modeling

A schematic diagram of the considered geometry is shown in Fig. 1. It consists of a backward-facing step in a duct where the step height is $h = 1$ cm. The coordinate system is defined as shown schematically in this figure, where the x_1- and x_2- coordinate directions denote, respectively, the streamwise and transverse directions. The upstream height is also $h = 1$ cm, hence

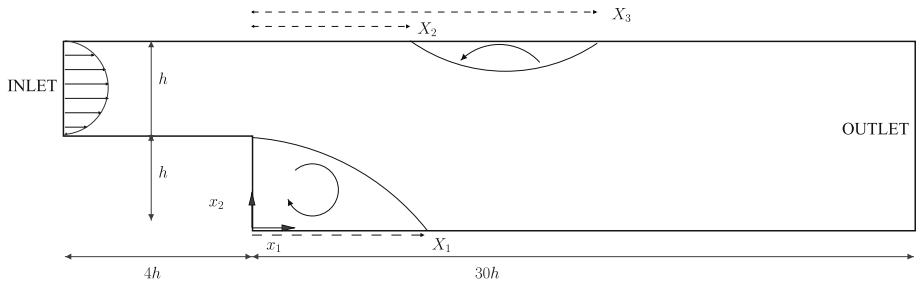

Fig. 1. The backward-facing-step scheme.

the downstream height is $2h$. The flow entering the channel is assumed to be fully developed and is described using u_1-velocity parabola for laminar flow. Barton [4] stated that when using an inlet channel upstream of the step, significant differences occur for low Reynolds numbers, however, they are localized in the sudden expansion region. In this study, to minimize its possible effect on the numerical solution, it has been decided to use an inlet length of $4h$. After the step, physically the flow needs some streamwise distance to adjust and become fully developed. For that reason, the downstream region length has been taken equal to $30h$. The outflow boundary condition was applied at the exit channel $x_1 = 30h, x_2 = [0 : 2h]$. The inlet velocity profile is prescribed on $\partial\Omega_1$ (i.e. for $x_1 = -4h, x_2 = [h : 2h]$) to

$$\begin{cases} \bar{u}_1(-4h, x_2) = \frac{4}{3}\frac{Re_v}{h^3}(x_2 - h)(2h - x_2), \\ \bar{u}_2(-4h, x_2) = 0. \end{cases} \tag{27}$$

On all other boundaries a null velocity is prescribed.

The chosen fluid assumed to be Newtonian and incompressible is air with dynamic viscosity μ and density ρ, respectively, equal to 1.81×10^{-5} kg/(m s) and 1.205 kg/m^3. The mean velocity U_∞ at the inlet is chosen such that the flow is driven at given Reynolds numbers $Re = \frac{U_\infty D_h}{v}$ (where $v = \frac{\mu}{\rho}$ and $D_h = 2h$) that lead to stable flows. Many authors such as Gresho et al. [31], Gartling [1] concluded that it is possible to obtain a steady solution for this flow until $Re = 800$. Other authors such as Barkley et al. [32] continued this stability analysis up to $Re = 1500$ and stated that the flow remains stable. As far as we are concerned, the range for the Reynolds number between 100 and 800 has been chosen such that the flow remains stable for sure.

In order to apply the model reduction eight velocity fields have been computed (i.e. $K = 8$ in (17)) from $Re = 100$ to $Re = 800$ by step 100. For all Reynolds number being tested, downstream of the step, there was a main recirculation region, whose length increased with the Reynolds number (Fig. 2). For a Reynolds number equal to 400, a second recirculation bubble appears attached to the upper wall of the channel. Fig. 2 presents the evolution of non-dimensioned lengths X_1/h, X_2/h and X_3/h with respect to the Reynolds number from 100 up to 800. This figure also compares our results to those from [33–35]. The results follow the trend as observed in the literature.

4.2. Adaptation of the general reduced model formulation for the backward-facing step problem

The prescribed input velocity $\bar{u}_1$ being an explicit function of the location x_2 and of the Reynolds number Re (see (27)), one has $u_1(-4h, x_2) = f(x_2)Re$ and $u_2(-4h, x_2) = 0$. Hence, the introduction of these relationships into (14) gives

$$\begin{cases} X + \Omega Z(X) + G'Re + G^+ = 0, \\ Y - HX = 0, \end{cases} \tag{28}$$

where the vector G' involved in (28) is in $\mathbb{R}^{d\times N}$. In the case of the backward-facing step, there is no additional Dirichlet condition, nor non-null fluxes to be considered added to the set of input. Hence, the vector G^+ involved in (28) is not considered

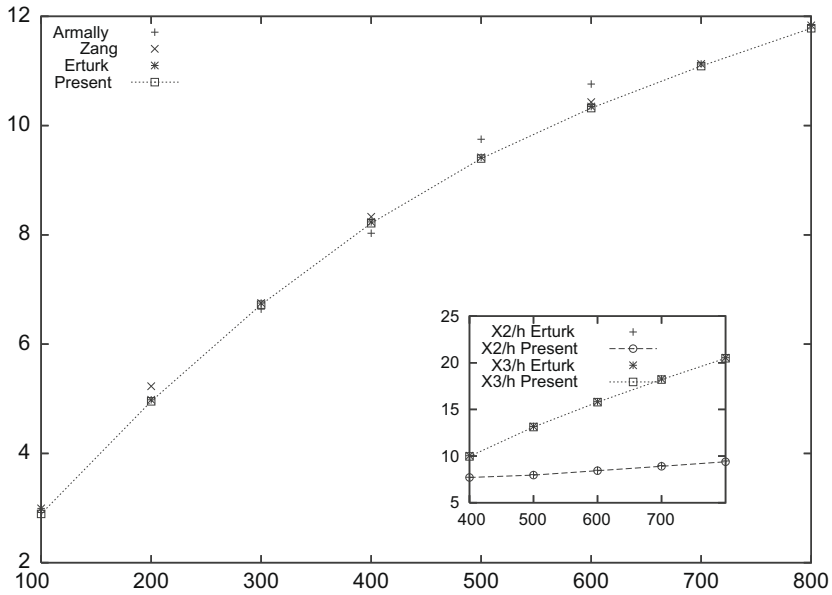

Fig. 2. Size of the main recirculation region length X_1/h as a function of the Reynolds number Re. The locations of the detachment point X_2/h and the reattachment point X_3/h as a function of the Reynolds number Re are shown in the inset.

in this special case. In the developed identification method, one uses this formulation as the structure for the reduced model to be identified. Thus, the reduced model structure is

$$\begin{cases} \dot{x} + \omega Z(x) + gRe = 0, \\ \widetilde{Y} - hx = 0, \end{cases}$$

where the input matrix g is, in this special case, a vector. The method described in Section 3.2 is applied on this new formulation for the reduced model. Two test cases, each one involving a specific set of output, will be considered: the first one includes almost the whole velocity field, the second one includes only a given velocity profile. In order to obtain the data from the detailed model, and after mesh convergence tests, a total number of nodes equal to 144,247 were necessary to obtain accurate and stable results.

4.3. Case one

In this first test case, all the nodes whose x_1- coordinate is included between the $x_1/h = -2$ and the $x_1/h = 30$ range are included in the reduction process. This gives a total number of 139,677 nodes in total. The maximum order for model reduction is seven so that the identification is performed in an over-determined way.

4.3.1. The reduced model identification

Table 1 gives the evolution of the cost function, the mean quadratic errors σ and the maximum error ε (defined, respectively, in (29) and (30)) with respect to the reduced model order. The mean quadratic errors and maximal errors are defined distinctly for velocity components u_1 and u_2 since the order of magnitude of both are very different. In order to compare these error results with the order of magnitude of the velocities, we present in Table 2 the magnitude of the velocities data, where the mean value represents the statistical mean of data. This table also presents the identification time needed to identify the reduced model for each order. The identification software was programmed with the Fortran 90 language and run on a dual-core bi-processor AMD Opteron 2.2 GHz with 3 Go of RAM on a HP DL 145G2 data processing server

$$\sigma_{u_i} = \left. \sqrt{\frac{1}{K \times q} \mathcal{J}} \right|_{u_i}, \tag{29}$$

$$(\varepsilon_{u_i})_{\max} = \left. \sup_{\substack{j=1,\dots,K \\ k=1,\dots,q}} |hx - Y^*| \right|_{u_i}. \tag{30}$$

Fig. 3 presents the evolution of the cost function value $\mathcal{J}$ (defined by (17)) as a function of the increasing reduced model order and, for each order, the decreasing cost function value with respect to the inner iterations (see Algorithm 1). This figure shows that for a given order the cost function is still decreasing and that the cost function value is generally decreasing with respect to the reduced model order at the end of the optimization iterations. The peaks appearing at the beginning of iterations at a given order are due to the non-perfect initialization of the data.

Table 1
Evolution of the cost function value $\mathcal{J}$, the mean quadratic errors $\sigma_{u_i}, i = 1,2$ the maximum errors $\varepsilon_{u_i}, i = 1,2$ and the identification computation time with respect to the reduced model order n.

Order	$\mathcal{J}$	σ_{u_1}	ε_{u_1}	σ_{u_2}	ε_{u_2}	CPU (s)
1	$4.96 \times 10^{+2}$	2.92×10^{-2}	1.31×10^{-1}	1.62×10^{-4}	4.22×10^{-2}	$4.60 \times 10^{+0}$
2	$7.22 \times 10^{+1}$	1.09×10^{-2}	4.95×10^{-2}	9.92×10^{-5}	1.89×10^{-2}	$6.42 \times 10^{+1}$
3	$1.33 \times 10^{+1}$	4.63×10^{-3}	2.36×10^{-2}	6.44×10^{-5}	9.02×10^{-3}	$1.51 \times 10^{+2}$
4	$2.18 \times 10^{+0}$	1.84×10^{-3}	1.28×10^{-2}	4.06×10^{-5}	5.52×10^{-3}	$2.19 \times 10^{+2}$
5	4.09×10^{-1}	7.80×10^{-4}	3.71×10^{-3}	2.64×10^{-5}	2.41×10^{-3}	$5.74 \times 10^{+1}$
6	5.51×10^{-2}	2.79×10^{-4}	1.44×10^{-3}	1.58×10^{-5}	1.03×10^{-3}	$4.14 \times 10^{+2}$
7	4.80×10^{-3}	8.15×10^{-5}	4.91×10^{-4}	8.54×10^{-6}	3.39×10^{-4}	$1.94 \times 10^{+2}$

Table 2
Mean and maximal velocities for both components u_1 and u_2.

	Max	Mean
u_1	8.76×10^{-1}	1.73×10^{-1}
u_2	1.04×10^{-1}	4.95×10^{-3}

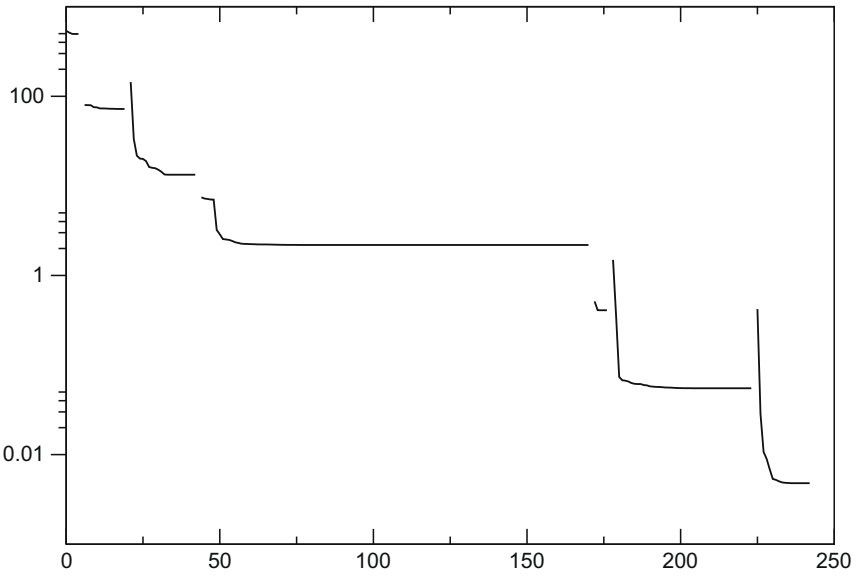

Fig. 3. Evolution of the cost function value $\mathcal{J}$ with respect to the optimization iterations for reduced model orders increasing until $n = 7$. Test case one.

4.3.2. Validation

The aim here is to validate the reduced model and to find out if the identified reduced model is able to reproduce with accuracy the output Y of the original detailed model when other Reynolds numbers are prescribed. According to Table 1, it can be seen that the best minimization is obtained for order 7, i.e. the cost function $\mathcal{J}$ and associated errors σ_{u_i} and ε_{u_i} are the lowest and actually low when compared to the mean and maximal velocities presented in Table 2.

Table 3 presents the validation results, i.e. the low mean quadratic errors σ_{u_i} and the low maximum absolute errors ε_{u_i} for both velocity components u_1 and u_2. Table 4 compares the length of the main recirculating region X_1/h obtained through the detailed model and through the reduced order model of order 7. Tables 5 and 6 give the detachment and reattachment locations of the first recirculation bubble on the upper wall X_2/h and X_3/h computed through both the detailed model and the reduced order one. Tables 4–6 show that the identified reduced model of order 7 is able to predict with accuracy the formation of the bubbles, the length of the main recirculating region X_1/h, and is also able to predict the apparition of the second recirculation region on the upper wall for $Re \geqslant 400$ along with the locations of the detachment and reattachment points.

Figs. 4 and 5 compare, respectively, the u_1 and u_2 velocity fields computed through both the detailed model and the reduced model of order 7. These figures show a good agreement of the velocity fields given by the detailed model (top) and the reduced model of order 7 (bottom).

Table 3
Evolution of errors σ_{u_i} and ε_{u_i}, $i = 1, 2$ for the seven considered validation test, i.e. for Reynolds numbers from 150 to 750 by steps of 100.

Re	σ_{u_1}	σ_{u_2}	ε_{u_1}	ε_{u_2}
150	3.98×10^{-4}	2.23×10^{-4}	2.27×10^{-3}	1.44×10^{-3}
250	2.06×10^{-4}	1.20×10^{-4}	1.05×10^{-3}	7.15×10^{-4}
350	1.25×10^{-4}	7.47×10^{-5}	5.34×10^{-4}	3.82×10^{-4}
450	5.81×10^{-5}	3.55×10^{-5}	2.82×10^{-4}	1.81×10^{-4}
550	5.77×10^{-5}	2.74×10^{-5}	2.56×10^{-4}	1.47×10^{-4}
650	1.35×10^{-4}	6.78×10^{-5}	5.00×10^{-4}	3.19×10^{-4}
750	2.57×10^{-4}	1.26×10^{-4}	1.00×10^{-3}	6.09×10^{-4}

Table 4
Length of the main recirculating region X_1/h obtained with on one hand the detailed model and, on the the other hand, the identified reduced model of order 7.

Re	$(X_1/h)_{DM}$	$(X_1/h)_{RM}$	Error %
150	3.962	4.038	1.917
250	5.872	5.841	0.514
350	7.507	7.450	0.748
450	8.843	8.770	0.819
550	9.885	9.809	0.767
650	10.71	10.67	0.438
750	11.44	11.39	0.459

Table 5
Detachment locations of the first recirculation bubble on the upper wall, X_2/h.

Re	$(X_2/h)_{DM}$	$(X_2/h)_{RM}$	Error %
450	7.769	8.215	5.733
550	8.190	8.503	3.821
650	8.663	8.982	3.682
750	9.145	9.423	3.035

Table 6
Reattachment locations of the first recirculation bubble on the upper wall, X_3/h.

Re	X_3/h_{DM}	X_3/h_{RM}	Error %
450	11.633	11.290	2.951
550	14.478	14.281	1.359
650	17.011	16.727	1.668
750	19.361	19.069	1.510

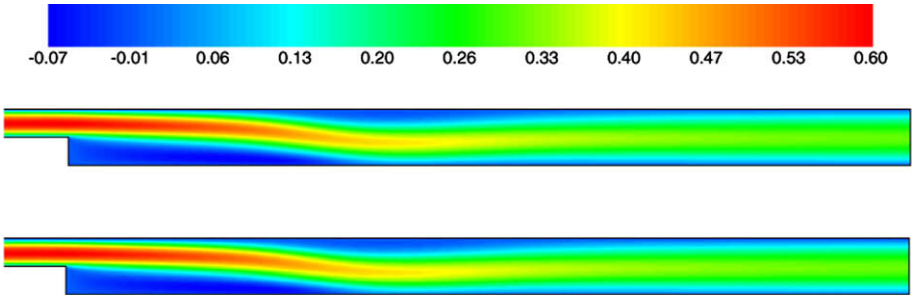

Fig. 4. Horizontal velocity field for both the detailed model (top) and the reduced model of order 7 (bottom).

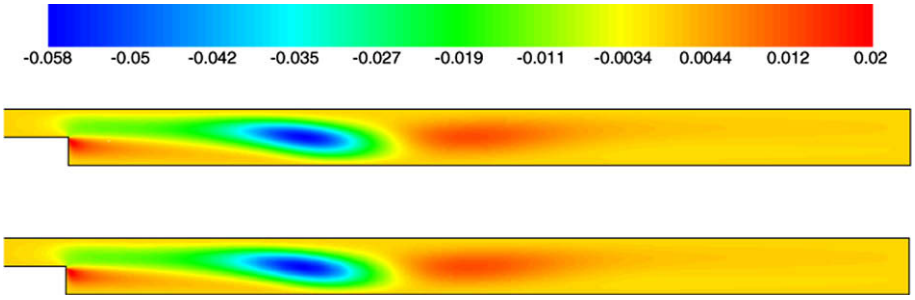

Fig. 5. Vertical velocity field for both the detailed model (top) and the reduced model of order 7 (bottom).

In Figs. 6 and 7, we plotted, respectively, the horizontal velocity u_1 and the vertical velocity u_2 profiles at $x_1/h = 6$, $x_1/h = 14$ and $x_1/h = 30$ locations. It can be seen that the profiles computed with the reduced model of order 7 are in very good agreement with those computed with the detailed model. Figs. 8 and 9 present, respectively, the stream function and the vorticity fields computed through both the detailed model and the reduced one of order 7. It can be seen a very good agreement between these results. Due to the spatial discretization of the velocity field that is obtained through the reduced model, the results are better on the stream function than for the vorticity. This is due to the fact that the stream function is obtained from an integration of the velocity field, whereas the vorticity is obtained through a space differentiation of the velocity field. The vorticity field is thus highly sensitive to any error on the solution when the space discretization is fine. On the contrary, the integration of the velocity field plays as a filter, and thus the stream function field is more continuous than the vorticity field.

4.3.3. Comparison of reduction modeling with a linear interpolation

In this section, we compare the results provided by the reduced model with those obtained classically through a linear interpolation. We again use the reduced model of order 7 identified and presented in the above sections. The principle of

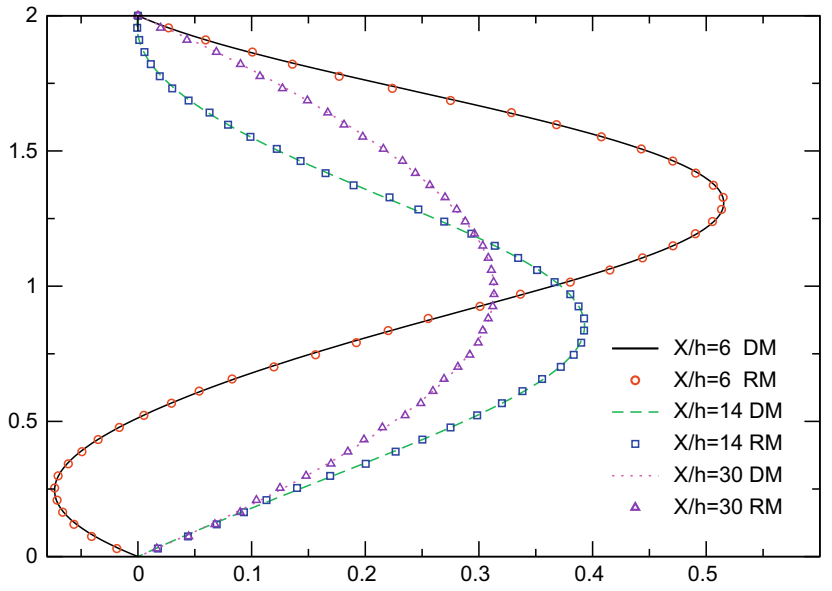

Fig. 6. Comparison of the detailed model with the reduced model of order 7: horizontal velocity u_1 for $Re = 550$.

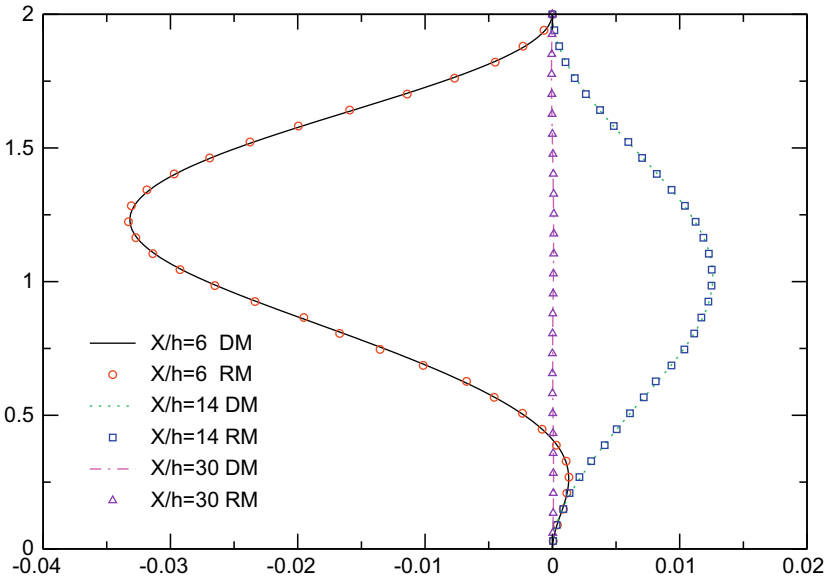

Fig. 7. Comparison of the detailed model with the reduced model of order 7: vertical velocity u_2 for $Re = 550$.

linear interpolation is very simple. If we call $\boldsymbol{u}(\boldsymbol{x}, Re)$ the velocity field for a Reynolds number Re included within the range $[Re^-; Re^+]$, then the procedure is simply

$$\boldsymbol{u}(\boldsymbol{x}, Re) = \boldsymbol{u}(\boldsymbol{x}, Re^-) + \frac{\boldsymbol{u}(\boldsymbol{x}, Re^+) - \boldsymbol{u}(\boldsymbol{x}, Re^-)}{Re^+ - Re^-} \cdot (Re - Re^-).$$

The linear interpolation method has been applied for seven Reynolds numbers from 150 to 750 by steps of 100, with seven Re^- from 100 to 700 by steps of 100 and seven Re^+ from 200 to 800 by steps of 100.

The accuracy of the fields provided by the classical interpolation procedure are presented in terms of quadratic errors σ_{u_i} and maximum absolute errors ε_{u_i} in Table 7. The comparison of these results with those related to the identified reduced model (see Table 3) shows that the reduced order model is much more able to predict the velocity field at a different Reynolds number than the classical interpolation procedure.

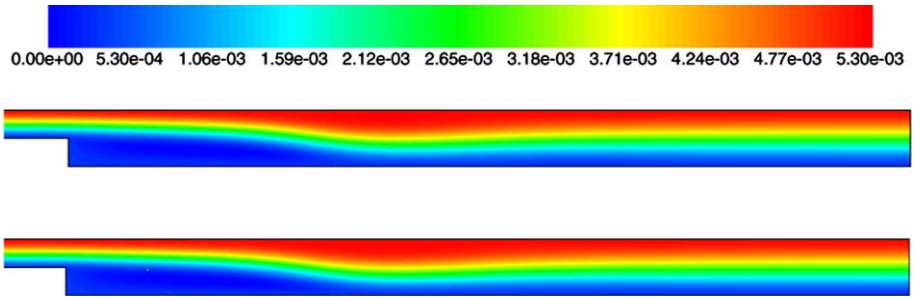

Fig. 8. Stream function fields of the detailed model (top) and of the reduced model of order 7 (bottom) for $Re = 550$.

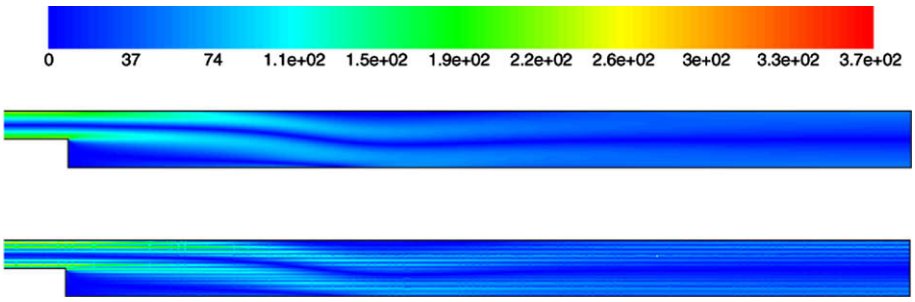

Fig. 9. Vorticity fields of the detailed model (top) and of the reduced model of order 7 (bottom) for $Re = 550$.

Table 7
Evolution of errors interpolation σ_{u_i} and ε_{u_i}, $i = 1, 2$ for the seven considered validation test: *Re* from 150 to 750 by steps of 100.

Re	σ_{u_1}	σ_{u_2}	ε_{u_1}	ε_{u_2}
150	1.547×10^{-3}	4.891×10^{-4}	7.321×10^{-3}	2.774×10^{-3}
250	1.573×10^{-3}	4.771×10^{-4}	7.328×10^{-3}	2.480×10^{-3}
350	1.618×10^{-3}	4.883×10^{-4}	7.279×10^{-3}	2.432×10^{-3}
450	1.641×10^{-3}	4.804×10^{-4}	6.880×10^{-3}	2.392×10^{-3}
550	1.673×10^{-3}	4.606×10^{-4}	6.790×10^{-3}	2.424×10^{-3}
650	1.758×10^{-3}	4.642×10^{-4}	7.377×10^{-3}	2.621×10^{-3}
750	1.846×10^{-3}	4.844×10^{-4}	8.033×10^{-3}	2.895×10^{-3}

4.4. Case two

In this second test case, we used a specific set of outputs where we considered only 135 nodes located on the $x_1/h = 9$ line. Eight direct detailed model runs (from $Re = 100$ to $Re = 800$ by steps of 100) were again performed to form the output vector Y^*. The maximum order for model reduction is thus seven so that the identification is performed in an over-determined way.

4.4.1. The reduced model identification

Fig. 10 presents the evolution of the cost function value $\mathcal{J}$ (defined by (17)) as a function of the increasing reduced model order and, for each order, the decreasing cost function value with respect to the inner iterations (see Algorithm 1). This figure shows that for a given order the cost function is still decreasing and that the cost function value is generally decreasing with respect to the reduced model order at the end of the optimization iterations. The peak appearing at the beginning of the optimization iterations for the seventh order is due to the non-perfect initialization of the data.

Table 8 gives the evolution of the cost function $\mathcal{J}$, the mean quadratic errors σ and the maximum error ε with respect to the reduced model order. We observe a drastic decrease of the cost function and of the identification errors (σ and ε) with respect to the reduced model order. Furthermore, the errors are very low when compared to the velocity magnitudes (see Table 2 for comparison).

4.4.2. The reduced model validation

The aim here is to validate the reduced model and to find out if the identified reduced model is able to reproduce with accuracy the output Y of the original detailed model when other Reynolds numbers are prescribed. We again chose to use the

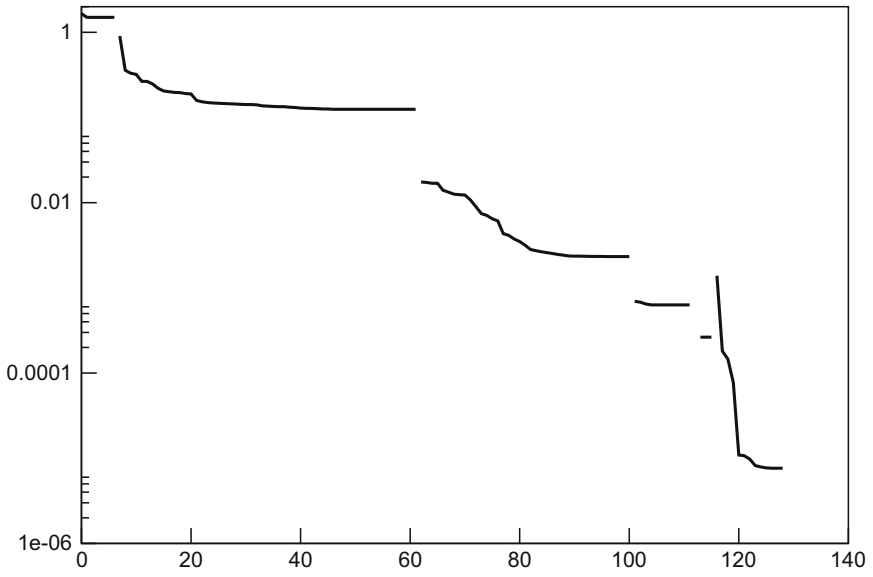

Fig. 10. Evolution of the cost function value $\mathcal{J}$ with respect to the optimization iterations for reduced model orders increasing until $n = 7$. Test case two.

Table 8
Evolution of the cost function value $\mathcal{J}$, the mean quadratic errors $\sigma_{u_i}, i = 1,2$ the maximum errors $\varepsilon_{u_i}, i = 1,2$ and the identification computation time with respect to the reduced model order n.

Order	$\mathcal{J}$	σ_{u_1}	ε_{u_1}	σ_{u_2}	ε_{u_2}	CPU (s)
1	$1.50 \times 10^{+0}$	5.17×10^{-2}	1.38×10^{-1}	6.92×10^{-3}	2.46×10^{-2}	1.10×10^{-2}
2	1.25×10^{-1}	1.34×10^{-2}	3.51×10^{-2}	3.52×10^{-3}	1.79×10^{-2}	3.96×10^{-1}
3	2.33×10^{-3}	1.58×10^{-3}	5.74×10^{-3}	1.21×10^{-3}	3.61×10^{-3}	3.25×10^{-1}
4	6.32×10^{-4}	8.77×10^{-4}	2.38×10^{-3}	9.01×10^{-4}	2.20×10^{-3}	2.66×10^{-1}
5	2.64×10^{-4}	6.61×10^{-4}	1.79×10^{-3}	7.82×10^{-4}	6.66×10^{-4}	2.90×10^{-2}
6	2.64×10^{-4}	6.61×10^{-4}	1.79×10^{-3}	7.82×10^{-4}	6.66×10^{-4}	6.70×10^{-2}
7	7.64×10^{-6}	5.19×10^{-5}	1.46×10^{-4}	2.19×10^{-4}	3.05×10^{-4}	2.91×10^{-1}

Table 9
Evolution of errors σ_{u_i} and $\varepsilon_{u_i}, i = 1,2$ for the seven considered validation test: Re from 150 to 750 by steps of 100.

Re	σ_{u_1}	σ_{u_2}	ε_{u_1}	ε_{u_2}
150	2.16×10^{-4}	1.30×10^{-4}	4.21×10^{-4}	2.50×10^{-4}
250	1.92×10^{-4}	6.01×10^{-5}	3.62×10^{-4}	1.07×10^{-4}
350	2.06×10^{-4}	3.11×10^{-5}	3.59×10^{-4}	6.18×10^{-5}
450	2.57×10^{-4}	1.05×10^{-4}	4.25×10^{-4}	2.13×10^{-4}
550	3.30×10^{-4}	1.73×10^{-4}	5.69×10^{-4}	3.47×10^{-4}
650	5.97×10^{-4}	2.87×10^{-4}	9.99×10^{-4}	5.68×10^{-4}
750	3.46×10^{-3}	1.39×10^{-3}	5.58×10^{-3}	2.51×10^{-3}

Table 10
Mean and maximal velocities for the components u_1 and u_2.

	Max	Mean
u_1	7.37×10^{-1}	1.71×10^{-1}
u_2	7.79×10^{-2}	4.95×10^{-3}

seven-order reduced model for validation. The chosen Reynolds numbers are taken from 150 to 750 by steps of 100. Table 9 reports the results of validation, i.e. the low mean quadratic errors σ_{u_i} and the low maximum absolute errors ε_{u_i} for both velocity components u_1 and u_2. Table 9 clearly shows that the errors are low when compared to the order of magnitude of the maximal and mean value of velocity components reported in Table 10. We also point out that the CPU time of simulation of the reduced model is less than 10^{-3} s.

5. Conclusion

In this study, a model reduction was carried out on laminar steady incompressible fluid flows by using an identification technique derived from the Modal Identification Method. A general formulation derived from the finite element method could lead to consider a general formulation for fluid flows. The matrix structure has been established for the Navier–Stokes problem in a general manner for the transient case. After writing these equations in the modal basis, and then in the stationary case, the matrix formulation with specific terms to treat the boundary condition has been formulated.

The identification procedure works as an inverse problem of parameter estimation. The outer loop increases the reduced model order. For each reduced model order, the optimization algorithm consists in minimizing a cost function that integrates the differences between the results given by the reduced model and the ones given by the original detailed model. The cost function is minimized using a gradient-type method where the gradient is computed through the adjoint (co-state) equation.

The results presented in this paper show that the reduced model accuracy increases with the model order. The identified reduced order model has been validated computing the reduced model with Reynolds numbers that were not used for the reduction process. We found that the identified reduced order model was able to predict with accuracy the x_1- and x_2- velocities, the stream function field and, to a lesser extent, the vorticity field. The reduced model could also be validated comparing the results for the length of the first recirculation bubble, and the locations of the detachment and reattachment of the second recirculating bubble appearing attached to the top wall for Reynolds number around 400. All these results are in very good agreement with those taken from the related literature.

We point out that two very distinct cases have been tested. The first is more classical since we considered almost the whole velocity field as output data needed for model reduction. The second case is more original since we selected only the velocities located on a single transverse line. This leads to consider a very efficient reduction tool when dealing only on a part of the flow. Note that such an approach is not possible with other techniques such as the POD for instance. For both test cases, a reduced order model could be identified and validated in a satisfying way with tests based on computations with other Reynolds numbers than the ones used for the identification process.

Let us underline two features very interesting when using the reduced order model through the identification method. At first, the velocity fields are computed very quickly with the reduced model. The CPU time needed to access the solution is of the order of magnitude of the millisecond. Next, the reduced model is computed by solving a nonlinear stationary system while most CFD packages use a non-stationary scheme for solving a stationary Navier–Stokes problem.

We point out that this reduction process is at present efficient on low Reynolds numbers with simple two dimensional laminar flows where the velocity fields can be retrieved very accurately. The natural extension of the proposed work concerns the application of the developed algorithms for fluid flows around cylinders with the Von–Karmàn structures. The other field in which we are interested in concerns the coupling of such Navier–Stokes problems with heat exchange. Though the gradient-type optimization algorithms were well suited for the presented model identification, the use of zero-order optimization algorithm should be compulsory for more complicated cases where the cost function may present several unknown local minima due to more complex physics and couplings. The preliminary tests would lead to consider the genetic algorithms and especially the particle swarms algorithms for the non-convex optimizations. Next, we plan to use such reduced models for control, e.g. temperature control. This step will concern the numerical implementation of control algorithms, leaning on the previously obtained reduced model, to realize a real thermal controlled system. The control goal can be, for instance, to follow prescribed temperatures on several given locations or to minimize (or maximize) heat transfer along some walls. In the framework of boundary control, the control parameters are the boundary conditions of the system, i.e. the velocity for the fluid mechanics point of view and a heat flux or a prescribed temperature for the thermal point of view.

Acknowledgment

The authors would like to thank Professor E. Erturk for very kindly providing his numerical data that were used for comparison between his models and our reduced order models on the backward-facing step.

References

[1] D.K. Gartling, A test problem for outflow boundary conditions – flow over a backward-facing step, International Journal of Numerical Methods in Fluids 11 (1990) 953–967.
[2] J. Kim, P. Moin, Application of a fractional-step method to incompressible Navier–Stokes equations, Journal of Computational Physics 59 (1985) 308–323.
[3] G. Comini, M. Manzan, C. Nonino, Finite element solution of the stream function-vorticity equations for incompressible two-dimensional flows, International Journal of Numerical Methods in Fluids 19 (1994) 513–525.
[4] I.E. Barton, The entrance effect of laminar flow over a backward-facing step geometry, International Journal of Numerical Methods in Fluids 25 (1997) 633–644.
[5] B.C. Moore, Principal component analysis in linear systems: controllability, observability and model reduction, IEEE Transactions on Automatic Control 26 (1981) 17–32.
[6] M.T. Ben Jaafar, R. Pasquetti, D. Petit, Model reduction for thermal diffusion: application of the Eitelberg, Marshall and aggregation methods to a heat transmission tube model, International Journal of Numerical Methods in Engineering 29 (1990) 599–617.
[7] J.L. Lumley, Stochastic Tools in Turbulence, vol. 12, Academic Press, New York, 1970.

[8] A.J. Newman, Model reduction via the Karhunen–Loève expansion Part I, II, Technical Report, Technical Report of the Institute for Systems Research, University of Maryland, 1996.
[9] L. Sirovich, Empirical Eigen Functions and Low Dimensional Systems, New Perspectives in Turbulence, Springer-Verlag, 1991.
[10] D. Petit, R. Hachette, D. Veyret, A modal identification method to reduce a high order model: application to heat conduction modelling, International Journal of Modelling and Simulation 17 (1997) 242–250.
[11] Y. Favennec, M. Girault, D. Petit, The adjoint method coupled with the modal identification method for nonlinear model reduction, Inverse Problems in Science and Engineering 14 (2006) 153–170.
[12] O. Balima, Y. Favennec, D. Petit, Model reduction for heat conduction with radiative boundary conditions using the modal identification method, Numerical Heat Transfer Part B 52 (2007) 107–130.
[13] O. Balima, Y. Favennec, M. Girault, D. Petit, Comparison between the modal identification method and the POD-Galerkin method for model reduction in nonlinear diffusive systems, International Journal of Numerical Methods in Engineering 67 (2006) 895–915.
[14] F. Hecht, C. Parés, Nsp1b3: un logiciel pour eésoudre les équations de Navier Stokes incompressible 3D, Technical report, INRIA's research report 1449, 1991.
[15] O. Pironneau, Finite Element Methods for Fluids, Wiley, Chichester, 1989.
[16] K. Ito, S.S. Ravindran, Optimal control of thermally convected fluid flows, SIAM Journal on Scientific Computing 6 (1998) 1847–1869.
[17] K. Ito, S.S. Ravindran, A reduced-order method for simulation and control of fluid flows, Journal of Computational Physics 143 (1998) 403–425.
[18] P. Oswald, Remarks on multilevel bases for divergence-free finite elements, Numerical Algorithms 27 (2) (2001) 131–152.
[19] J.E. Roberts, J.-M. Thomas, Mixed and hybrid methods, Handbook of Numerical Analysis, vol. 2, North-Holland, 1993.
[20] F. Hecht, O. Pironneau, A. Le Hyaric, K. Ohtsuka, Freefem++ manual, version 2.0-0, 2005.
[21] W.H. Schilders, H.A. Vorst, J. Rommes, Model Order Reduction: Theory Research Aspects and Applications, Springer-Verlag, Berlin Heidelberg, 2008.
[22] B.S. Liao, Z. Bai, W. Gao, The important modes of subsystems: a moment-matching approach, International Journal for Numerical Methods in Engineering 70 (2007) 1581–1597.
[23] L. Tartar, An Introduction to Navier–Stokes Equation and Oceanography, Springer-Verlag, Berlin Heidelberg, 2006 (Lecture Notes of the Unione Matematica Italiana).
[24] O. Balima, Y. Rouizi, Y. Favennec, D. Petit, Reduced modelling through identification on 2-D incompressible laminar flows, in: Proceedings Inverse Problems, Design and Optimization Symposium, 2007.
[25] P.E. Gill, W. Murray, M.H. Wright, Practical Optimization, Academic Press, London, 1992.
[26] J.L. Lions, Contrôle optimal de systèmes gouvernés par des équations aux dérivées partielles, Dunod, Paris, 1968.
[27] F.X. Le Dimet, J. Blum, Assimilation de données pour les fluides géophysiques, MATAPLI, Bull. SMAI, 67:35–55, January 2002.
[28] O. Balima, Y. Rouizi, Y. Favennec, D. Petit, A. Charette, Reduced modelling through identification on 2-D incompressible laminar flows, Inverse Problems in Science and Engineering, 2009, Special Issue: Inverse Problems, Design and Optimization (IPDO2007) Symposium, Miami Beach, Florida, USA, April 16–18, 2007.
[29] Y. Favennec, V. Labbé, F. Bay, Induction heating processes optimization – a general optimal control approach, Journal of Computational Physics 187 (2003) 68–94.
[30] Y. Favennec, Optimization and adjoint state, Thermal measurements and inverse techniques: a tool for the characterization of multiphysical phenomena, Lecture in Eurotherm Winter School METTI 2005. <http://www.let.ensma.fr/ASO/FAVENNEC>.
[31] P.M. Gresho, D.K. Gartling, J.R. Torczynski, K.A. Cliffe, K.H. Winters, T.J. Garrat, A. Spence, J.W. Goodrich, Is the steady viscous incompressible two-dimensional flow over a backward facing step at Re = 800 stable?, International Journal of Numerical Methods in Fluids 17 (1993) 501–541
[32] D. Barkley, M.G.M. Gomes, R.D. Henderson, Three-dimensional instability in flow over a backward-facing step, Journal of Fluid Mechanics 473 (2002) 167–190.
[33] E. Erturk, Numerical solutions of 2-D steady incompressible flow over a backward-facing step, Part I: high Reynolds number solutions, Computers & Fluids 37 (6) (2008) 633–655.
[34] B.F. Armally, F. Durst, J.C.F. Pereira, B. Schonung, Experimental and theoretical investigation of backward-facing step flow, Journal of Fluid Mechanics 127 (1983) 473–496.
[35] Y. Zang, R.L. Street, J.R. Koseff, A non-staggered grid, fractional step method for time-dependent incompressible Navier–Stokes equations in curvilinear coordinates, Journal of Computational Physics 114 (1994) 18–33.